Anomalous scaling corrections and quantum phase diagram of the Heisenberg antiferromagnet on the spatially anisotropic honeycomb lattice

Alexander Sushchyev and Stefan Wessel

Institute for Theoretical Solid State Physics, RWTH Aachen University, JARA Fundamentals of Future Information Technology and JARA Center for Simulation and Data Science, 52056 Aachen, Germany

Using large-scale quantum Monte Carlo simulations, we determine the ground state phase diagram of the spin-1/2 antiferromagnetic Heisenberg model on the honeycomb lattice for the most generic case of three varying interaction strengths along the different lattice directions. We identify continuous quantum phase transition lines that separate the long-range ordered antiferromagnetic regime from three distinct quantum-disordered phases, each characterized by dominant dimer-singlet formations. The finite-size behavior along these phase transition lines exhibits anomalously large corrections to scaling, which we relate to similar recent findings in certain dimerized quantum spin systems and to singular one-dimensional limits in the model parameter space. We also comment more generally on the nonuniversality of critical cumulant ratios in anisotropic systems and attempts to restore universality by varying the aspect ratio.

I. INTRODUCTION

The honeycomb lattice has the lowest possible coordination number ($z = 3$) among the eleven uniform Archimedean tilings (i.e., periodic tessellations of the plane by regular polygons such that all edge lengths are equal and every vertex looks alike) [1]. Nevertheless, its bipartite character still allows for the stabilization of a Néel antiferromagnetic (AFM) ground state—realized, e.g., in the spin-1/2 Heisenberg antiferromagnet with isotropic nearest-neighbor interactions, i.e., considering equal interaction strengths among all the bonds of the honeycomb lattice [2,3]. However, upon increasing the interaction strength along one of the three inequivalent bond directions with respect to the other two, such a quantum spin system can be driven out of the AFM regime. More specifically, it has been shown that once the corresponding coupling ratio extends beyond about 1.735, the AFM order is replaced by a nonmagnetic, quantum disordered ground state, characterized by the dominant formation of singlets among the nearest-neighbor bonds with the larger coupling strength [4]. This way of dimerizing the honeycomb lattice is similar to models of dimerized quantum magnets on the square lattice. In the latter case, different dimerization patterns, such as columnar vs staggered dimerization, have been intensively investigated recently [4–11]. In particular, for the specific case of a staggered dimerization large corrections to scaling have been reported at the quantum phase transition that separates the AFM phase from the quantum disordered regime [7–11]. These scaling corrections have been associated to certain nontopological cubic terms in the effective low-energy field theory describing the quantum critical point [9]. Apparently, they give rise to a further weakly irrelevant operator [11], in addition to those expected for the three-dimensional classical Heisenberg universality class that generically characterizes the quantum phase transitions in such bipartite dimerized spin systems [12].

Here, we report that similar anomalously large scaling corrections also appear in the dimerized Heisenberg model on the honeycomb lattice. Moreover, in this case, we can link the estimated subleading scaling correction to the *leading* scaling correction in a special, one-dimensional limit of the Heisenberg model on the honeycomb lattice. The latter is accessible upon considering the most generic case, in which all three inequivalent nearest-neighbor bonds on the honeycomb lattice have a different coupling strength. In order to analyze this quantum spin system, we used large-scale quantum Monte Carlo (QMC) simulations, based on the stochastic series expansion (SSE) method [13–15]. From the QMC analysis of these quantum phase transitions, we then obtain the global ground state phase diagram of this most generic form of the nearest-neighbor spin-1/2 Heisenberg model on the honeycomb lattice with three different interaction strengths. Certainly, in view of the abundant realizations of the honeycomb lattice geometry in magnetic compounds, this more generic quantum phase diagram is of value on its own.

The remainder of this paper is organized as follows. In Sec. II, we introduce the model Hamiltonian and comment on the employed QMC approach. Next, we present the ground state phase diagram as obtained from QMC simulations in Sec. III. A detailed finite-size analysis of the anomalous scaling corrections is provided in Sec. IV, focusing on the Binder ratio [11,16]. We finally comment more generally on the nonuniversality of such critical cumulant ratios for anisotropic systems in Sec. V, before final conclusions are drawn in Sec. VI.

II. MODEL AND METHOD

In the following, we consider the spin-1/2 Heisenberg model on the honeycomb lattice, taking into account three different exchange couplings J_1, J_2, and J_3 along the three inequivalent nearest-neighbor bond directions, as indicated in
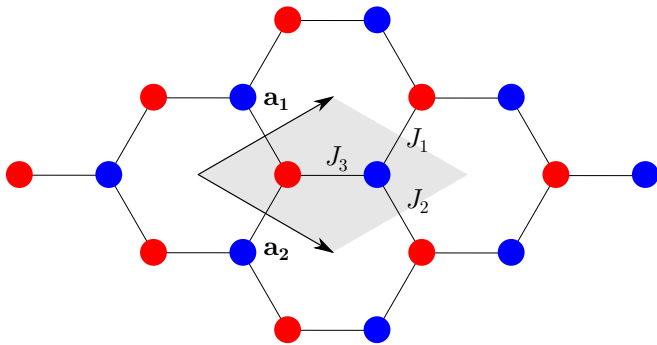
FIG. 1. Illustration of the honeycomb lattice with its bipartite structure, as indicated by two differently colored lattice sites. Also indicated is the unit cell spanned by the lattice vectors $\mathbf{a}_1$ and $\mathbf{a}_2$ as well as the exchange couplings J_1, J_2, and J_3 for the Heisenberg model along the three inequivalent bond directions. The shown finite lattice corresponds to $L = 3$.

Fig. 1 (we consider antiferromagnetic exchange interactions, $J_1, J_2, J_3 \geqslant 0$). This system is described by the Hamiltonian

$$H = J_1 \sum_{\langle i,j \rangle_1} \mathbf{S}_i \cdot \mathbf{S}_j + J_2 \sum_{\langle i,j \rangle_2} \mathbf{S}_i \cdot \mathbf{S}_j + J_3 \sum_{\langle i,j \rangle_3} \mathbf{S}_i \cdot \mathbf{S}_j, \quad (1)$$

where each of the three summations extends only over the parallel bonds corresponding to the labeling in Fig. 1. From previous studies it is well established that in the isotropic case, $J_1 = J_2 = J_3$, the ground state exhibits long-range AFM order, with a staggered magnetization m_s^{iso} that is reduced by about 54% from its classical value in the perfect Néel state [3]. Upon enhancing one of the three exchange couplings, e.g., considering $J_1 > J_2 = J_3$, the AFM order gets suppressed, and for $J_1/J_2 = J_1/J_3 > 1.735(1)$ the ground state becomes the aforementioned dimerized quantum disordered state with a dominant singlet formation along the J_1 bonds [4]. We denote this regime by D_1 in the following. Correspondingly, upon increasing J_2 (J_3) with respect to $J_1 = J_3$ ($J_1 = J_2$), we obtain dimerized phases with dominant singlet formations along the J_2 (J_3) bonds, which we denote by D_2 (D_3). In the following, we explore the phase diagram for the more general case in which the system is fully spatially anisotropic, i.e., all three couplings may be varied independently.

In order to extract the ground state properties of this system, we performed large-scale QMC simulations based on the SSE method with directed loop updates. We consider finite-size systems of rhombic shape as indicated in Fig. 1, denoting by L the extent of the system in both the $\mathbf{a}_1$ and $\mathbf{a}_2$ directions, so that the number of spins $N = 2L^2$. Furthermore, we employ periodic boundary conditions and performed the QMC simulations at sufficiently low temperatures to probe ground state properties. Based on the staggered structure factor

$$S_{AF} = \frac{1}{N} \sum_{i,j} \epsilon_i \epsilon_j \mathbf{S}_i \cdot \mathbf{S}_j, \quad (2)$$

where $\epsilon_i = \pm 1$, depending on the sublattice on which $\mathbf{S}_i$ is located, we can estimate the staggered magnetization
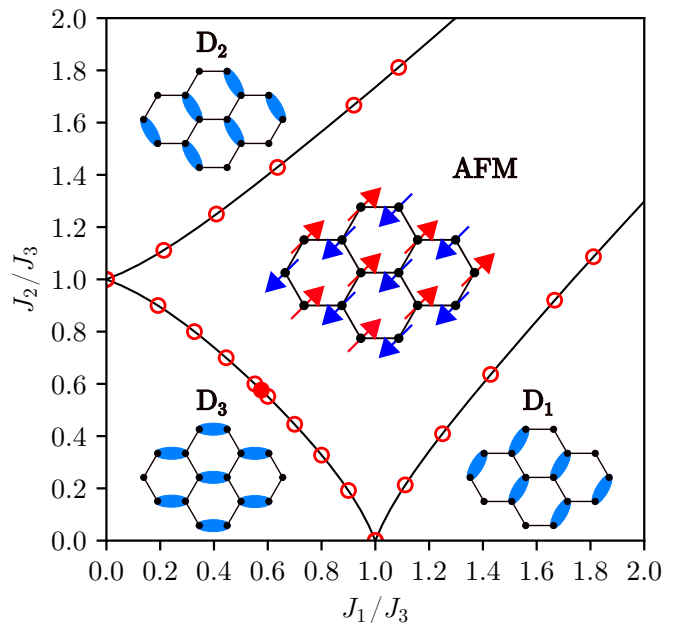
$$m_s = \sqrt{S_{AF}/N} \quad (3)$$

FIG. 2. Ground state phase diagram of the spin-1/2 Heisenberg model on the honeycomb lattice, expressed in the two parameter ratios J_1/J_3 and J_2/J_3. Circles indicate results from QMC simulations, while the solid line is a guide to the eye. Illustrated within each quantum disordered regime is the dominant dimerization pattern.

after an extrapolation to the thermodynamic limit. Furthermore, as detailed below, we can extract the phase transition lines out of the AFM regime upon measuring the Binder ratio [4,11,16]

$$R = \frac{\langle M_s^4 \rangle}{\langle M_s^2 \rangle^2}, \quad (4)$$

where $M_s = \sum_i \epsilon_i S_i^z$ denotes the staggered moment. In the following section, we first present the resulting phase diagram of the Hamiltonian H before we discuss the QMC-based determination of the phase boundaries in Sec. IV.

III. GROUND STATE PHASE DIAGRAM

We first consider a parametrization in units of the coupling J_3, i.e., tuning the ratios J_1/J_3 and J_2/J_3. From the finite-size analysis of the QMC data, detailed in the next section, we then obtain the ground state phase diagram shown in Fig. 2, which also illustrates the different ground states. An alternative form of the phase diagram, adapted to its symmetries, is obtained upon expressing it in terms of barycentric coordinates, defined as $j_i = J_i/(J_1 + J_2 + J_3)$, such that $j_1 + j_2 + j_3 = 1$. The resulting phase diagram is shown in Fig. 3. Included in this figure is the value of the staggered magnetization m_s inside the AFM phase, normalized to its maximum value m_s^{iso} in the isotropic case (located at the center of the triangle).

From these ground state phase diagrams, we find that the three distinct quantum disordered regimes D_1, D_2, and D_3 are generically separated by the AFM phase, as they meet only pairwise at singular points that are located on special lines where one coupling strength vanishes. For example, for $J_1 = 0$, the system decouples into zig-zag chains (cf.
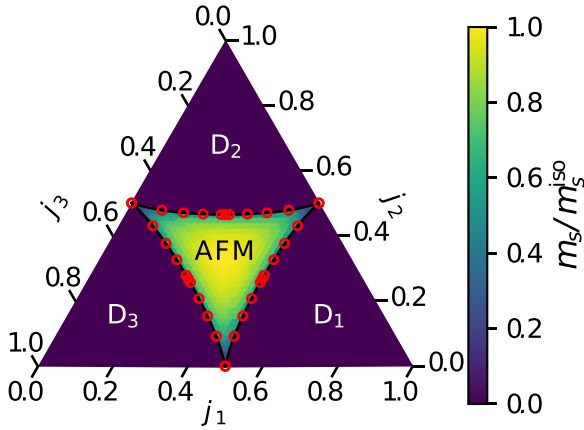
FIG. 3. Ground state phase diagram of the spin-1/2 Heisenberg model on the honeycomb lattice, expressed in barycentric coordinates. Circles indicate results from QMC simulations, while the solid line is a guide to the eye. Also shown inside the AFM regime is the magnitude of the staggered magnetization m_s, normalized to its maximum value m_s^{iso} in the isotropic case (located at the center of the triangle).

Fig. 1) that are aligned along the $\mathbf{a}_2$ direction. If $J_2 = J_3$, these spin-1/2 Heisenberg chains have a gapless, quantum critical ground state, and an arbitrarily weak interchain coupling $J_1 > 0$ drives the system into the AFM regime [17]. However, for $J_2 > J_3$ ($J_3 > J_2$) the isolated chains have a gapped ground state, with dominant singlet formations along the J_2 (J_3) bonds, corresponding to the one-dimensional limit of the D_2 (D_3) phase [17]. In the latter case, a finite interchain coupling $J_1 > J_1^c > 0$ is therefore required to close the excitation gap and drive the system into the AFM regime. This quasi-one-dimensional physics, along with the corresponding cases for $J_2 = 0$ and $J_3 = 0$, gives rise to the curved triangular shape of the AFM regime in Fig. 3.

In the following section, we provide a detailed finite-size analysis of the Binder ratio, based on which the above phase boundaries were obtained. In particular, we show that the Binder ratio exhibits anomalous finite-size corrections which can be linked to the above mentioned singular points.

IV. FINITE-SIZE ANALYSIS

In order to determine the stability range of the AFM regime, we typically fixed in the QMC simulations the value of J_2/J_3 and varied J_1/J_3, i.e., we probed the system along horizontal cuts in Fig. 2. Indeed, we can furthermore restrict ourselves to the regime $J_1 \leqslant J_2 \leqslant J_3$, as other sections of the AFM boundary can be obtained after appropriate relabelings of the coupling constants.

However, here we first consider the symmetric line along which $J_1 = J_2$. Figure 4 shows the dependence of the Binder ratio R on the coupling ratio J_1/J_3 along this diagonal. As a dimensionless quantity, R is particularly useful for finite-size studies of (quantum) critical phenomena, since to leading order it exhibits a crossing point at the (quantum) critical point when considering different finite-size systems with a fixed spatial (as well as—for quantum phase transitions—the
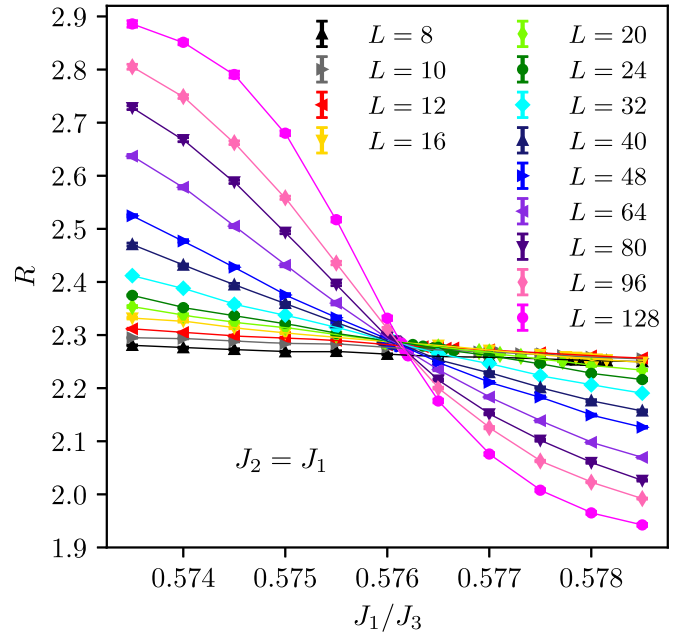

FIG. 4. Binder ratio R as a function of $J_1 = J_2$ for different system sizes L.

space-time) aspect ratio. Here, we consider $L \times L$ lattices and fix the inverse temperature $\beta = 2L$ (in units of $1/J_3$) [11].

The QMC data for R in Fig. 4 indeed cross for different system sizes near $J_1/J_3 \approx 0.576$. However, closer inspection reveals that there is a systematic drift of the crossing points between different system sizes and we therefore need to examine in more detail the crossing point values of $g = J_1/J_3$ and R between system sizes L and $2L$ in Fig. 5 and Fig. 6, respectively.
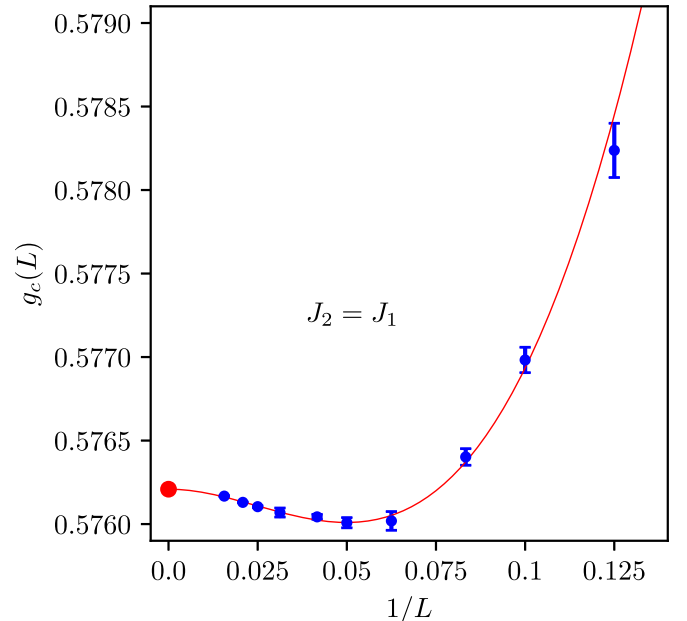

FIG. 5. Crossing point values of $g = J_1/J_3$ for the Binder ratio R for $J_2 = J_1$ between system sizes L and $2L$. Also included is a fit to the finite-size scaling form (5).
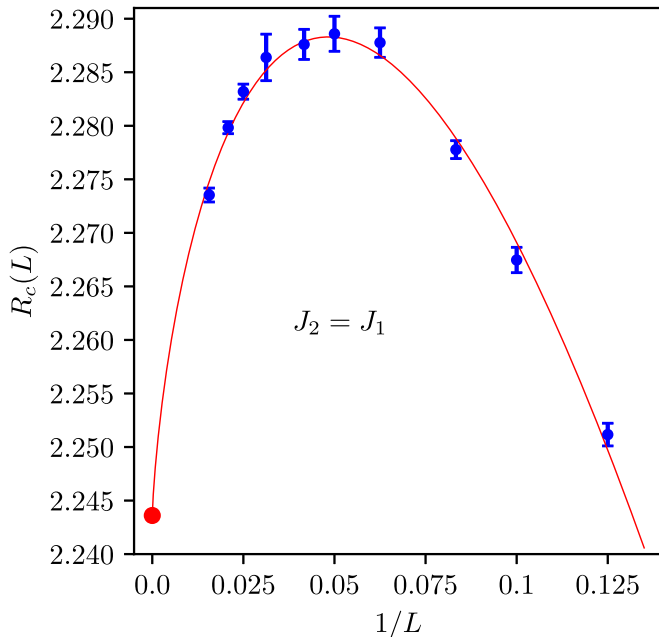
FIG. 6. Crossing point values of the Binder ratio R for $J_2 = J_1$ between system sizes L and $2L$. Also included is a fit to the finite-size scaling form (6).
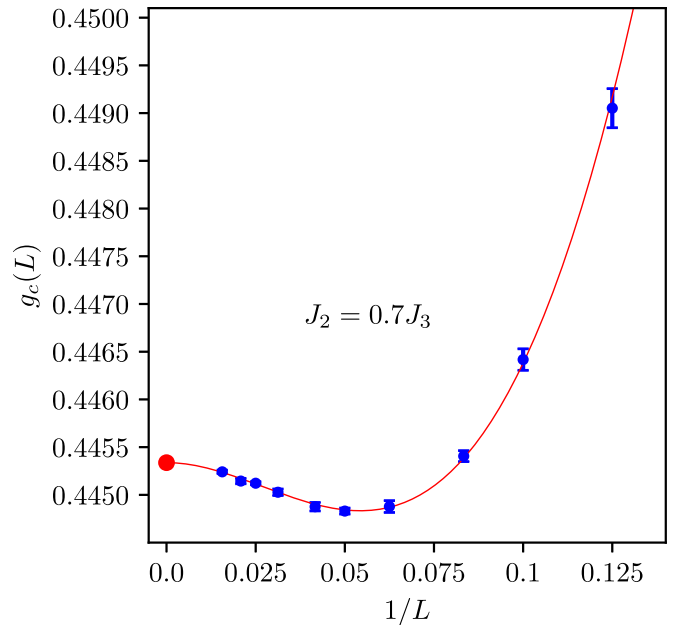

FIG. 7. Crossing point values of $g = J_1/J_3$ for the Binder ratio R for $J_2 = 0.7J_3$ between system sizes L and $2L$. Also included is a fit to the finite-size scaling form (5).

A striking feature of the finite-size dependence of both quantities is a strongly nonmonotonic behavior, similar to the one observed for the staggered dimer square-lattice model (but not for the columnar dimer case) in Ref. [11]. This similarity may not come as a surprise if one compares the two lattice structures: also for the honeycomb lattice, the stronger bonds (in this case the J_3 bonds) are arranged in a staggered fashion (but with fewer interdimer couplings than for the staggered dimer square lattice). We note that such a nonmonotonic behavior was however not reported in Ref. [4], possibly due to (i) a lower resolution in scanning the coupling ratio near the quantum critical point for the large system sizes than here and/or (ii) the different finite-size lattice geometry employed in that study.

In Ref. [11], a careful finite-size analysis of such nonmonotonic scaling corrections was performed. It was concluded that they are best accounted for by considering *two* subleading correction terms to the leading scaling form,

$$g_c(L) = g_c + L^{-1/\nu}(a_1 L^{-\omega_1} + a_2 L^{-\omega_2}), \quad (5)$$

$$R_c(L) = R_c + b_1 L^{-\omega_1} + b_2 L^{-\omega_2}, \quad (6)$$

where g denotes the tuning parameter that drives the quantum phase transition (here, $g = J_1/J_3$), ν is the correlation length scaling exponent, and ω_1 and ω_2 are two correction exponents (the a_i, b_i are nonuniversal prefactors). For the quantum phase transition under consideration here as well as in Ref. [11], $1/\nu = 1.406$ and $\omega_1 = 0.78$ can be taken from the classical values of the three-dimensional Heisenberg universality class [18–20] (note that, besides ν, also the correction exponent ω_1 is universal within a given universality class). Furthermore, Ref. [11] estimated a value of $\omega_2 \approx 1.25$ for the staggered dimer square-lattice model. This value is greater than ω_1 and smaller than $2\omega_1$, i.e., ω_1 is still the

leading scaling correction, related to the three-dimensional classical Heisenberg universality class. The further correction term, related to ω_2, was argued to steam from the cubic term in the effective action of the field theory describing the quantum critical point [9,11].

We find that the above extended scaling ansatz also fits well (i.e., with values of $\chi^2/\mathrm{DOF} \approx 1$) to the anomalous, nonmonotonic behavior that we observe for the honeycomb lattice model: fits to the QMC data based on this ansatz are included in Fig. 5 and Fig. 6 (unfortunately, the accessible accuracy on the estimated crossing points does not allow us to robustly estimate the exponents independently). Based on these fits, we furthermore obtain an estimate for the critical coupling $J_1^c = 0.57620(1)J_3$ (shown in Fig. 2 and Fig. 3 by the full circle) and $R_c = 2.244(1)$, which are in accord with earlier estimates [4] along the symmetric line (the stated uncertainties refer to the performed fits and do not account for the unknown uncertainty in the value of ω_2 estimated in Ref. [11]). We find that the above anomalous finite-size behavior persists also away from the symmetric line. As a further example, we discuss here $J_2 = 0.7J_3$. In this case, fits to the data shown in Figs. 7 and 8 lead to $J_1^c = 0.44533(1)J_3$ and $R_c = 2.258(1)$, respectively.

By contrast, we observe a rather distinct finite-size scaling behavior if we fix the coupling ratio to $J_2 = J_3$. In this case, the data shown in Figs. 9 and 10 does not feature the above nonmonotonic behavior; instead it fits well to scaling forms with only a single exponent each, which we denote by p and ω, respectively,

$$g_c(L) = g_c + a L^{-p}, \quad (7)$$

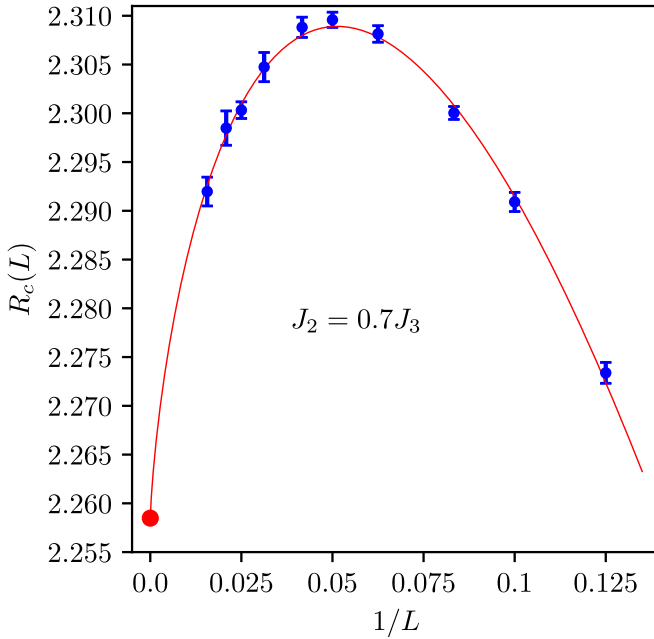$$R_c(L) = R_c + b L^{-\omega}. \quad (8)$$

FIG. 8. Crossing point values of the Binder ratio R for $J_2 = 0.7J_3$ between system sizes L and $2L$. Also included is a fit to the finite-size scaling form (6).

FIG. 10. Crossing point values of the Binder ratio R for $J_2 = J_3$ between system sizes L and $2L$. Also included is a fit to the finite-size scaling form (8).

The extracted value of $J_1^c = 0.001(1)J_3$ in this case is consistent with zero and thus in accord with the quasi-one-dimensional physics mentioned in the previous section. Indeed, also the extracted value of $R_c = 2.996(2)$ is compatible with the value of $R_c = 3.05(5)$ that we obtain from QMC simulations performed for an isolated spin-1/2 Heisenberg chain (cf. Appendix).
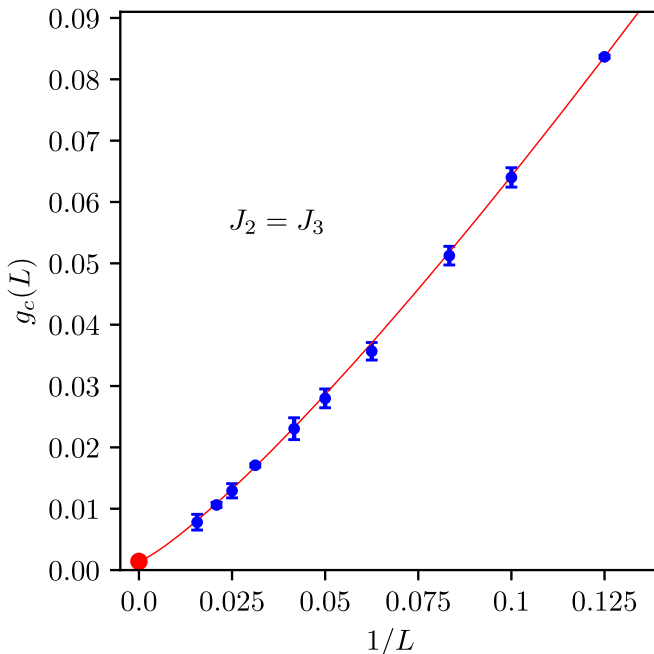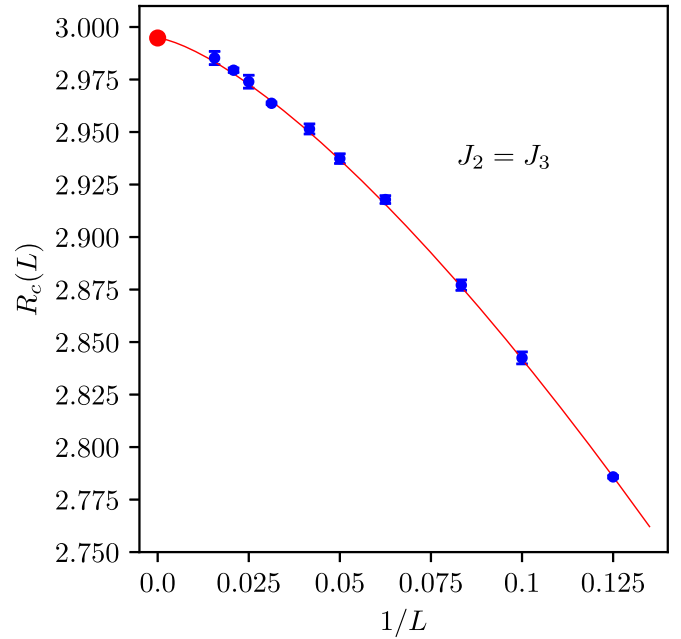

FIG. 9. Crossing point values of $g = J_1/J_3$ for the Binder ratio R for $J_2 = J_3$ between system sizes L and $2L$. Also included is a fit to the finite-size scaling form (7).

Furthermore, we find that the estimated values of the correction exponent $\omega \approx 1.40(4)$ as well as $p \approx 1.21(5)$ are comparable to the above cited estimate for ω_2, suggesting that the subleading scaling corrections, captured by the $L^{-\omega_2}$ term, may arise due to a simple crossover effect: for small system sizes, the finite-size behavior is still affected by the influence of the specific fixed point (in a renormalization-group sense), corresponding to the decoupled spin-1/2 Heisenberg chains. Only on sufficiently large system sizes does the actual asymptotic scaling of the three-dimensional classical Heisenberg universality class prevail. This scenario provides a natural explanation for the nonmonotonic finite-size behavior observed above (a crossover scale of $L_c \approx 20$ can then be estimated based on the local extrema in the finite-size crossing points). We comment further on this point and its relation to previous work in the final Sec. VI.

In Fig. 11, we summarize the extrapolated values of the critical Binder ratio R_c as a function of J_2 along the considered branch of the AFM phase boundary line. We observe a systematic dependence of the value of R_c on the coupling ratios, along with the approach towards 3 for $J_2 = J_3$. In particular, the values that we obtain for R_c are all substantially larger than the critical value $R_c^{\text{iso}} = 2.0437\ldots$ of the isotropic three-dimensional classical Heisenberg model. This property reflects the fact that the correlations in the considered quantum spin systems are not isotropic, a property that indeed affects the value of the critical Binder ratio [21,22]. We elaborate further on this point in the following section.

V. GENERAL REMARK ON ANISOTROPIC SYSTEMS

The fact that certain dimensionless quantities such as the critical Binder ratio R_c are not universal but depend on the anisotropy of the correlations [21,22] is indeed well
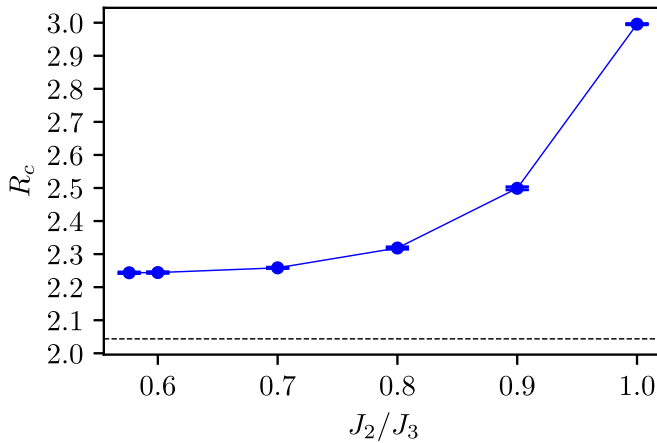
FIG. 11. Critical Binder ratio R as a function of J_2 along the considered phase transition line. The dashed line indicates the value of the critical Binder ratio $R_c^{iso} = 2.0437\ldots$ of the isotropic three-dimensional classical Heisenberg model.
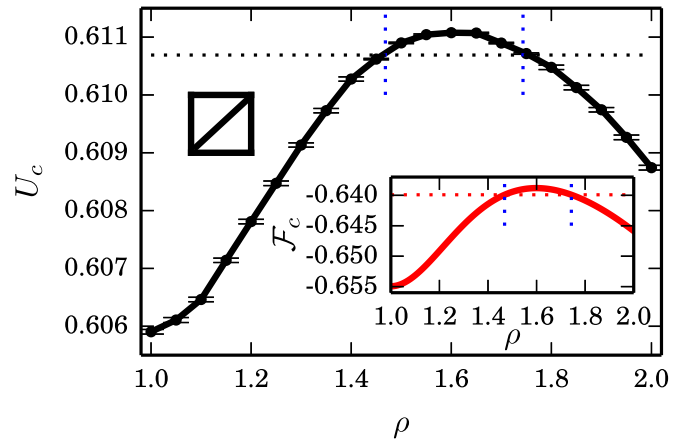

FIG. 12. Dependence of the critical Binder cumulant U_c (main panel) and the critical amplitude of the singular free energy density $\mathcal{F}_c$ (inset) on the aspect ratio ρ for the anisotropic Ising model with $E_3 = 3E$. Isotropic values are indicated by horizontal lines. Vertical lines indicate the two values of ρ^*. The left inset illustrates the unit cell with E_1, E_2, E_3 along horizontal, vertical, and diagonal directions, respectively.

established by now. It has been suggested [10] that the isotropic value R_c^{iso} may still be restored upon considering finite systems with an appropriate aspect ratio (even though such a restoration has been argued to not be crucial for the analysis of, e.g., the universal properties of the critical point [11]). More specifically, for the simple case of an underlying square lattice geometry, one would consider a finite rectangle with L_x (L_y) unit cells in the x (y) direction, such that, by tuning the aspect ratio $\rho = L_y/L_x$, the critical Binder ratio $R_c(\rho)$ takes on the isotropic value $R_c(\rho^*) = R_c^{iso}$ for an appropriate value of $\rho = \rho^*$, even when $R_c(1) \neq R_c^{iso}$ (for a quantum critical system, the inverse temperature has to be adapted correspondingly as well [10]). Such restorations have indeed been demonstrated for various classical and quantum models for which the principal axes of the correlation function align with the axes of the underlying square lattice [10,22–24]. For a general anisotropic two-dimensional system, the angular dependence of the correlations is given by the angle Ω, specifying the orientation of the two principal axes, and the ratio q of the two principal correlation lengths upon approaching criticality [25]. The above special cases correspond to $\Omega = 0$ or $\pi/2$. For example, in the first case, the value of ρ^* is fixed by the condition that $q\rho^* = 1$ (e.g., for $q = 2$, such that the correlation length in the x direction is twice the one along the y direction; this yields $\rho = 1/2$, i.e., $L_x = 2L_y$). Such systems were termed "virtual isotropic" [5,10].

It is not clear (i) whether such a restoration is also feasible at all in the more generic case, where Ω takes on different values, i.e., when the principle axes are not aligned with the lattice directions, and, if so, (ii) how to physically interpret the value of ρ^* in that case. In the following, we demonstrate explicitly for a basic classical model that such a restoration of the isotropic value is apparently still possible—however, the value of ρ^* appears in this case to be unrelated to the orientation of the underlying correlations.

For this purpose, we consider the triangular-lattice Ising model [25–28], defined by

$$H^{Is} = -\sum_i [E_1\sigma_i\sigma_{i+\hat{x}} + E_2\sigma_i\sigma_{i+\hat{y}} + E_3\sigma_i\sigma_{i+\hat{x}+\hat{y}}], \quad (9)$$

where $\sigma_i = \pm 1$ reside on a square lattice with horizontal, vertical, and (up-right) diagonal couplings E_1, E_2, $E_3 \geqslant 0$ (the unit cell is illustrated in the inset of Fig. 12). The condition for the critical temperature T_c, separating the low-T ferromagnetic phase from the paramagnetic regime, reads $\hat{S}_1\hat{S}_2 + \hat{S}_2\hat{S}_3 + \hat{S}_3\hat{S}_1 = 1$, where $\hat{S}_\alpha = \sinh(2E_\alpha/T_c)$ [29]. In the following, we focus on the symmetric case $E_1 = E_2 = E$, for which $\Omega = \pi/4$ and $q = 1/\hat{S}_3$ [25,28]. Furthermore, the correlations decay equally along the x and y directions in this case.

In Fig. 12 we report the ρ dependence of the critical Binder cumulant [16]

$$U_c = 1 - \frac{1}{3}R_c, \quad R_c = \frac{\langle M^4 \rangle}{\langle M^2 \rangle^2}, \quad (10)$$

where $M = \sum_i \sigma_i$, for the specific case of $E_3 = 3E$, as obtained using Wolff-cluster Monte Carlo simulations [30] at T_c, extracted for the thermodynamic limit. The value of U_c obtained for $\rho = 1$ agrees with an earlier study [22]. In contrast to the standard Ising model ($E_1 = E_2$, $E_3 = 0$), for which $U_c(\rho)$ monotonously decreases for $\rho > 1$ from the isotropic value $U_c^{iso} = 0.61069\ldots$ at $\rho = 1$ [23], here it exhibits a nonmonotonous behavior. In particular, the isotropic value is recovered at two specific values, $\rho^* \approx 1.47$ and 1.74. While there is no apparent relation of these numbers to the value of $q = 2.82843\ldots$, we find that within the numerical precision they do agree with the values of ρ for which the critical amplitude of the singular free energy density $\mathcal{F}_c(\rho)$ recovers its isotropic value $\mathcal{F}_c^{iso} = -0.639912\ldots$ [31]; cf. the inset of Fig. 12. For the latter quantity we can extract ρ^* using exact conformal field theory-based expressions for $\mathcal{F}_c$ [27,28]. For $E_3 = 3E$, we obtain $\rho^* = 1.4683\ldots$ and $1.7433\ldots$, respectively.

We made the above observations also at other ratios E_3/E (see also Ref. [24] for the case $E_3 = E$), yielding different values of ρ^* and suggesting that, interestingly, (i) it is feasible

within the considered anisotropic Ising model to restore the isotropic values of both the critical Binder cumulant and the critical amplitude of the singular free energy density upon varying the aspect ratio ρ, (ii) the corresponding value(s) of ρ^* for both quantities are very close—if not equal, and (iii) the value(s) of ρ^* are not obviously related to geometric properties of the anisotropic correlation functions for $\Omega \neq 0, \pi/2$. It would certainly be interesting to examine these points in more detail in the future, both for the triangular-lattice Ising model and on more general grounds.

For the purpose of the present discussion, the relevant conclusion is as follows. Once the principal axes are not aligned to the underlying lattice directions, one cannot expect to be able to relate, as in previous cases [10,22,23], the value of ρ^* directly to the correlation length ratio along the lattice directions (which equals 1 in the above considered Ising model cases, since $E_1 = E_2$) nor to the ratio q of the two principal correlation lengths. In particular, it is thus not clear how the procedure proposed in Ref. [10] for the automated location of ρ^* can be generalized to the fully anisotropic case.

VI. CONCLUSIONS

Based on large-scale quantum Monte Carlo simulations we determined the ground state phase diagram of the spin-1/2 Heisenberg model on the honeycomb lattice with spatially fully anisotropic nearest-neighbor exchange interactions. In addition to the AFM phase, three quantum disordered regimes have been identified, each characterized by a dominant dimer singlet formation along the strongest bonds. The disordered phases are generically separated by the AFM regime, but meet pairwise at three singular points in the extended parameter domain.

The generic quantum phase transition along the boundary line of the AFM regime exhibits nonmonotonic anomalous finite-size corrections, similarly to the previously investigated staggered dimer model [11]. Based on a scaling ansatz with two irrelevant scaling correction terms, this behavior could be well captured. The additional scaling correction is subdominant to the leading finite-size correction that relates to the three-dimensional O(3) universality class. Upon approaching the aforementioned singular points, the system decouples into parallel arrays of spin-1/2 Heisenberg (zig-zag) chains, for which a similar finite-size correction term was identified to *leading* order. This suggests a crossover scenario to explain the nonmonotonic finite-size effects.

It may be worthwhile to mention that the cubic interaction term that was previously proposed to underlie the anomalous scaling observed in the staggered dimer model [9] has a formal similarity with the topological θ term that is characteristic for the gapless state of the spin-1/2 Heisenberg chain [17]. For the future it would thus be interesting to explore if a similar link between the subleading scaling correction and the behavior at the one-dimensional singular points that we observe here also emerges in appropriate generalizations of the staggered dimer model.

Finally, we pointed out that previously proposed schemes [10] for the automated restoration of isotropic values of cumulant ratios upon varying the aspect ratio are not directly applicable to generic anisotropic systems, even in
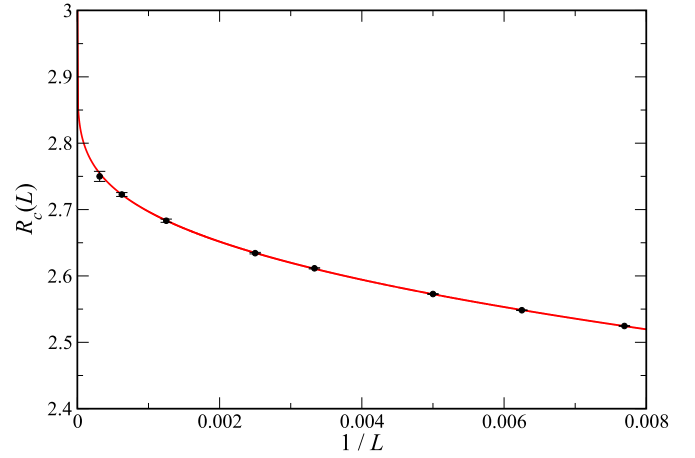

FIG. 13. Critical Binder ratio $R_c(L)$ for the spin-1/2 Heisenberg chain along with a fit to the finite-size scaling form (A1).

cases for which such a restoration may be feasible. Certainly, more work is required to explore the consequences of this observation.

APPENDIX: BINDER RATIO OF THE SPIN-1/2 HEISENBERG CHAIN

We performed QMC simulations for an isolated spin-1/2 Heisenberg chain in order to directly estimate the value of R_c at the singular points of the phase diagram. The results of these simulations are shown in Fig. 13, including data $R_c(L)$ for chains with L spins and periodic boundary conditions up to $L = 3200$, scaling the inverse temperature $\beta J = L$ in units of the nearest-neighbor exchange coupling J along the chain. We obtain a monotonous increase of $R_c(L)$ with increasing system size that fits well to a logarithmic finite-size dependence,

$$R_c - R_c(L) \propto [\ln(L)]^{-q}, \tag{A1}$$

and from performing a fit to the QMC data we obtain the estimates $R_c = 3.05(5)$ and $q = 1.1(1)$, respectively. Such a logarithmic finite-size behavior of $R_c(L)$ can be expected given that the asymptotic spin-spin correlation function of the spin-1/2 Heisenberg chain is well known to decay with distance r as $\sqrt{\ln(r)}/r$ [17], i.e., including a logarithm as well. We are not aware of any previous analytic prediction for the finite-size scaling form of the Binder ratio in this system.

[1] B. Grünbaum and G. C. Shephard, Math. Mag. **50**, 227 (1977).

[2] J. Richter, J. Schulenburg, and A. Honecker, in *Quantum Magnetism* (Springer, Berlin, 2004), pp. 85–153.

[3] U. Löw, Condens. Matter Phys. **12**, 497 (2009).

[4] F.-J. Jiang and U. Gerber, J. Stat. Mech.: Theory Exp. (2009) P09016.

[5] M. Matsumoto, C. Yasuda, S. Todo, and H. Takayama, Phys. Rev. B **65**, 014407 (2001).

[6] L. Wang, K. S. D. Beach, and A. W. Sandvik, Phys. Rev. B **73**, 014431 (2006).

[7] S. Wenzel, L. Bogacz, and W. Janke, Phys. Rev. Lett. **101**, 127202 (2008).

[8] F.-J. Jiang, Phys. Rev. B **85**, 014414 (2012).

[9] L. Fritz, R. L. Doretto, S. Wessel, S. Wenzel, S. Burdin, and M. Vojta, Phys. Rev. B **83**, 174416 (2011).

[10] S. Yasuda and S. Todo, Phys. Rev. E **88**, 061301(R) (2013).

[11] N. Ma, P. Weinberg, H. Shao, W. Guo, D.-X. Yao, and A. W. Sandvik, Phys. Rev. Lett. **121**, 117202 (2018).

[12] A. V. Chubukov, S. Sachdev, and J. Ye, Phys. Rev. B **49**, 11919 (1994).

[13] A. W. Sandvik and J. Kurkijärvi, Phys. Rev. B **43**, 5950 (1991).

[14] A. W. Sandvik, J. Phys. A: Math. Gen. **25**, 3667 (1992).

[15] A. W. Sandvik, Phys. Rev. B **59**, R14157 (1999).

[16] K. Binder, Z. Phys. B **43**, 119 (1981).

[17] T. Giamarchi, *Quantum Physics in One Dimension*, International Series of Monographs on Physics (Clarendon Press, London, 2004).

[18] R. Guida and J. Zinn-Justin, J. Phys. A: Math. Gen. **31**, 8103 (1998).

[19] M. Hasenbusch, J. Phys. A: Math. Gen. **34**, 8221 (2001).

[20] M. Campostrini, M. Hasenbusch, A. Pelissetto, P. Rossi, and E. Vicari, Phys. Rev. B **65**, 144520 (2002).

[21] X. S. Chen and V. Dohm, Phys. Rev. E **70**, 056136 (2004).

[22] W. Selke and L. N. Shchur, J. Phys. A: Math. Gen. **38**, L739 (2005).

[23] G. Kamieniarz and H. W. J. Blote, J. Phys. A: Math. Gen. **26**, 201 (1993).

[24] W. Selke, J. Stat. Mech.: Theory Exp. (2007) P04008.

[25] V. Dohm, Phys. Rev. E **100**, 050101(R) (2019).

[26] J. Stephenson, J. Math. Phys. **5**, 1009 (1964).

[27] V. Dohm and S. Wessel, Phys. Rev. Lett. **126**, 060601 (2021).

[28] V. Dohm, S. Wessel, B. Kalthoff, and W. Selke, J. Phys. A: Math. Theor. **54**, 23LT01 (2021).

[29] R. Houtappel, Physica **16**, 425 (1950).

[30] U. Wolff, Phys. Rev. Lett. **62**, 361 (1989).

[31] A. E. Ferdinand and M. E. Fisher, Phys. Rev. **185**, 832 (1969).